*Journal of Natural Disaster Science, Volume 35, Number 2, 2014, pp43-53*

# SEISMIC BEHAVIOR ANALYSIS OF MASONRY STRUCTURES USING THE DISTINCT ELEMENT METHOD CONSIDERING ELEMENT DEFORMABILITY

Aiko FURUKAWA*, Risa HORIKAWA**, Junji KIYONO***, and Kenzo TOKI****

*Associate Professor, Graduate School of Global Environmental Studies, Kyoto University
**Graduate Student, Dept. of Urban Management, Kyoto University
***Professor, Graduate School of Global Environmental Studies, Kyoto University,
****Professor, Research Center for Disaster Mitigation of Urban Cultural Heritage, Ritsumeikan University

(Received March 5, 2014 Accepted August 3, 2014)

**ABSTRACT**

In this study, we propose a new distinct element method (DEM) that considers element deformability for failure analysis of masonry structures. Many people in developing countries live in masonry structures. In earlier DEM schemes, a structure is modeled as an assembly of rigid elements, but element deformability cannot be considered. The deformation of a structure can be modeled by overlapping between elements, but Poisson's effect cannot be modeled. However, bricks used in developing countries can readily be deformed due to their low stiffness. Therefore, it is preferable to also consider element deformability in the DEM. In the new DEM, each element is divided into two parts: an inner part that considers deformation of the element itself, and an outer part that deals with contact between elements. Deformation of a structure can be modeled by overlapping between elements and deformation of the elements themselves. The validity of the method is confirmed through a comparison of the elastic deformation with a finite element model. It was found that the original DEM and the proposed method show different failure patterns of seismic behavior due to Poisson's effect.

**Keywords:** DEM, Element deformability, Masonry structure, Poisson's effect.

## 1. Introduction

The city of Bam in southeastern Iran was hit by a strong earthquake on December 26, 2003. About 43,200 people lost their lives [1], many due to the collapse of masonry buildings. Masonry structures are low-cost and construction practices are simple, so many people in developing countries live in such buildings. However, masonry structures are vulnerable to earthquakes. Therefore, the seismic collapse mechanisms of such structures need to be understood in order to develop effective reinforcement measures. To this end, the development of a numerical method that can accurately simulate the seismic behavior of masonry structures is needed.

There are two types of numerical simulation methods that can handle seismic behavior. One is based on continuum modeling, and the other, on discontinuum modeling.

Among numerical simulation methods, the finite element method (FEM) [2] is the most common technique for the analysis of a continuum. However, the FEM is based on the mechanics of the continuum and uses a continuous shape function, so it has difficulty in solving failure and collapse phenomena.

A new FEM, referred to as FEM-β, that can be regarded as a FEM with a special displacement field was proposed by Oguni et al. in 2004 [3]. In FEM-β, the continuous shape function is replaced by a discontinuous shape function, which enables it to solve failure phenomena. However, it does not model the re-establishment of contact between elements, so it cannot simulate collapse behavior.

A method based on discontinuum modeling is more suitable for simulating failure and collapse behaviors. The distinct element method (DEM) [4] is an established numerical simulation method for a discontinuum. In the DEM, a structure is modeled as an assembly of rigid elements, and a spring and dashpot are generated between two elements in contact. In the original DEM, there are no forces resisting tension between elements; therefore, it was impossible to simulate the behavior of a continuum. To give continuity to this discrete model, a spring that resists tension was added and this improved method is called the modified DEM (MDEM) [5] or the extended DEM (EDEM) [6]. In the MDEM and EDEM, the structure is modeled as an assembly of circular elements.

However, the elements are modeled as a rigid body, so deformation of the elements is not considered. Deformability of the structure can be modeled by overlapping between elements. Failure is modeled by breaking the spring. A method of determining the theoretical spring constant has not been established, so the value is generally determined experimentally or simply based on one-dimensional (1D) wave propagation equations. Therefore, the reliability of the results is not high.

A refined DEM [7] was then proposed by Furukawa et al. in 2011. In this scheme, a restoring spring resisting tension is included, the structure is modeled as an assembly of hexahedral elements, and the surface of each element is divided into many segments to which springs and dashpots are attached. This segmentation allows theoretical spring constants to be determined using three-dimensional (3D) stress-strain relationships. However, the elements are still modeled as a rigid body in the same way as in the original DEM, and the deformability of elements and Poisson's effect cannot be expressed. Because the bricks used in developing countries that we target in this study readily deform due to their low stiffness, it is preferable to consider the deformability of the elements themselves in the DEM. Therefore, we have developed a new DEM that considers the deformability of elements. The results of the new DEM are compared with those of the refined DEM to investigate the need to consider element deformability.

## 2. Refined DEM

### 2.1 Basic concept

Like the original DEM, the refined DEM models a structure as an assembly of rigid elements. The surface of an element is divided into many segments (**Fig. 1 (a)**), and a spring and a dashpot are attached to each segment (**Fig. 1 (b)**). Therefore, the elements have multiple springs on the surface. This segmentation of the surface allows the spring constant to be defined theoretically, which is the main improvement over earlier methods. For more details, see [7]. A restoring spring, which models the elasticity of the elements, is set between continuous elements (**Fig. 1 (c)**). Structural failure is modeled as breakage of the restoring spring, at which time the restoring spring is replaced with a contact spring and dashpot (**Fig. 1 (d)**). If two elements are initially continuous, the restoring spring is set between the elements until failure occurs. If these two elements recontact each other again after the failure, a contact spring and dashpot are set between the elements.

A contact spring and dashpot are used for simulating the contact, separation, and recontact between elements. The contact dashpots, which are set in parallel with the contact springs, are introduced to express energy dissipation due to the contact. Therefore, in the refined DEM, the spring constant can be derived theoretically, which makes the method suitable for simulating large displacement behaviors such as failure and collapse.

### 2.2 Analytical parameters

(1) Spring constant of each spring

A spring is attached to each surface segment. There are two types of springs: restoring springs and contact springs. Each spring constant is taken to have the same value. The springs are set for both the normal and shear direction of the surface. The spring constants per area, in both the normal and shear directions, are written as follows using the equilibrium of force for each pyramid (**Fig. 1 (e)**) composed of a

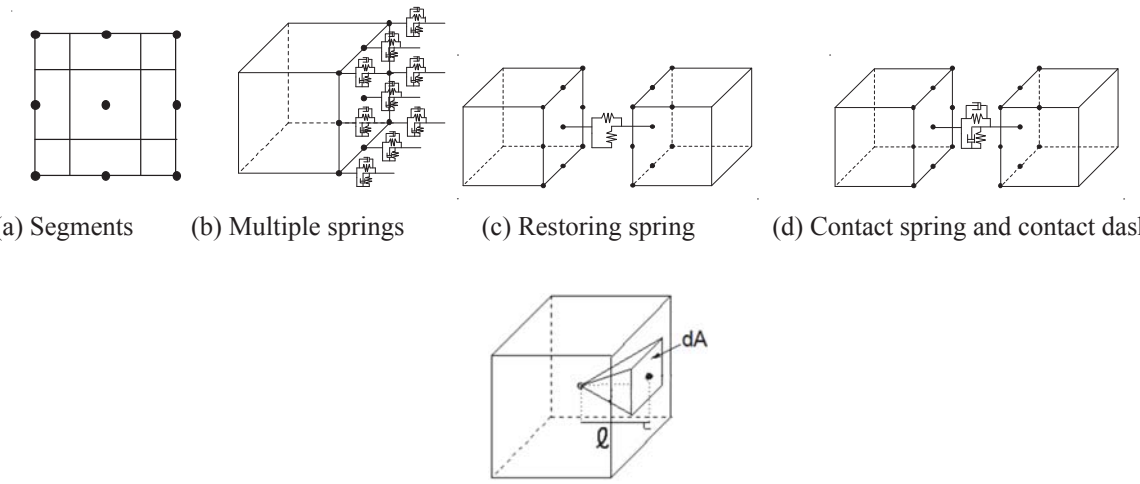


(a) Segments (b) Multiple springs (c) Restoring spring (d) Contact spring and contact dashpot

(e) Pyramid for deriving the spring constant

**Figure 1.** Modeling of a spring and dashpot in the refined DEM

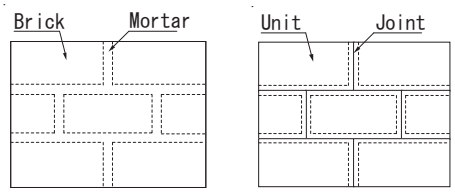


(a) Masonry structure (b) Analytical model

**Figure 2.** Modeling of a masonry structure

segment and the center of gravity for each element:

$$k_n = \frac{E}{(1-\nu^2)\ell}, \text{ and } \quad k_s = \frac{E}{2(1+\nu)\ell}, \tag{1}$$

where $E$ is Young's modulus and $v$ is Poisson's ratio for the element; $l$ is the distance from the surface to the center of gravity.

(2) Spring constant between elements

In the refined DEM, individual components of the masonry structure shown in **Fig. 2 (a)** are modeled in a simple manner, as shown in **Fig. 2 (b)**. The bricks themselves are modeled with rigid elements whereas the mortar joints between elements are modeled with multiple springs and dashpots. The size of one unit is the sum of the brick size and the mortar thickness. Each unit is modeled with one rigid element. The joints have zero thickness and are expressed by springs between the elements.

Two elements, A and B, are assumed to be continuous and connected to each other with mortar. Young's moduli are given by $E_A$ and $E_B$, and Poisson's ratios by $v_A$ and $v_B$ for elements A and B. The distances from each center of gravity to each segment are $l_A$ and $l_B$. For the mortar, Young's modulus and Poisson's ratio are $E_M$ and $v_M$, respectively, and $t_M$ is the mortar thickness. Assuming that the springs of elements A and B are connected in series, the spring constants between elements per area, $k_n$ and $k_s$, are found to be

$$\bar{k}_n = \frac{1}{\dfrac{\ell_A - t_M/2}{E_A/(1-\nu_A^2)} + \dfrac{t_M}{E_M/(1-\nu_M^2)} + \dfrac{\ell_B - t_M/2}{E_B/(1-\nu_B^2)}}, \text{ and}$$

$$\bar{k}_s = \frac{1}{\dfrac{\ell_A - t_M/2}{E_A/2(1+\nu_A)} + \dfrac{t_M}{E_M/2(1+\nu_M)} + \dfrac{\ell_B - t_M/2}{E_B/2(1+\nu_B)}}. \tag{2}$$

In the case where elements A and B are continuous and without mortar, the spring constants are written as

$$\bar{k}_n = \frac{1}{\dfrac{\ell_A}{E_A/(1-\nu_A^2)} + \dfrac{\ell_B}{E_B/(1-\nu_B^2)}}, \text{ and}$$

$$\bar{k}_s = \frac{1}{\frac{\ell_A}{E_A/2(1+\nu_A)} + \frac{\ell_B}{E_B/2(1+\nu_B)}}. \quad (3)$$

(3) Contact damping coefficient

If a segment of an element is in contact or in collision with another element with which the segment is not continuous via the restoring spring, a contact spring and dashpot are set between the elements. The contact dashpot is introduced to express the energy dissipation of the contact. The damping coefficient per area is calculated as follows:

$$c_n = 2h_n\sqrt{m_{ave}\bar{k}_n}, \quad c_s = 2h_s\sqrt{m_{ave}\bar{k}_s},$$
$$\text{and} \quad m_{ave} = \rho_A\ell_A + \rho_B\ell_B, \quad (4)$$

where $h_n$ and $h_s$ are the damping constants for the normal and shear directions, $m_{ave}$ is the equivalent mass per area relevant to this contact, and $\rho_A$ and $\rho_B$ are the mass densities of elements A and B.

### 2.3 Modeling of failure phenomena

Let $\sigma$ and $\boldsymbol{\tau}$ be the normal stress vector and shear stress vector acting at the contact point, and let $\mathbf{u}_n$ and $\mathbf{u}_s$ be the relative displacement vectors in the normal and shear directions between the segments. Stresses $\sigma$ and $\boldsymbol{\tau}$ are expressed as

$$\sigma = \bar{k}_n|\mathbf{u}_n| \quad \text{and} \quad \boldsymbol{\tau} = \bar{k}_s\mathbf{u}_s. \quad (5)$$

When the stresses acting on the spring reach their elastic limit, failure phenomena are expressed using the breakage of the restoring spring. The elastic limits are modeled using the criteria of tension, shear, and compression failure.

(1) Tension failure mode

When normal stress $\sigma$ exceeds tensile strength $f_t$, the restoring spring is assumed to be broken by tension failure. The yield function has the following form (**Fig. 3**):

$$f_1(\sigma) = \sigma - f_t. \quad (6)$$

(2) Shear failure mode

For assessment of shear failure, the Coulomb friction envelope is used. The yield function has the following form **(Fig. 3**):

$$f_2(\sigma) = |\boldsymbol{\tau}| + \sigma\tan\phi - c, \quad (7)$$

where $c$ is the bond strength and $\phi$ is the friction angle.

(3) Compression failure mode

For the compression failure mode, an ellipsoid cap model is used. The yield function has the following form that makes use of compressive strength $f_m$ and material model parameter $C_s$ (**Fig. 3**):

$$f_3(\sigma) = \sigma^2 + C_s|\boldsymbol{\tau}|^2 - {f_m}^2. \quad (8)$$

$C_s$ is based on past research on masonry structures [8].

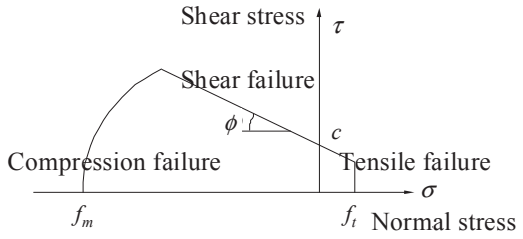


**Figure 3.** Modeling of failure phenomena

### 2.4 Nonlinearity of contact force

When a segment of an element is not continuous, but in contact (or recontact) with another element, a contact spring and contact dashpot are attached to each segment. The contact force is generated only while there is active compression force. The contact force in the shear direction is bounded by the friction limit. The friction limit is expressed by

$$|\boldsymbol{\tau}| = \sigma\tan\phi, \quad (9)$$

where $\phi$ is the friction angle.

### 2.5 Equations of motion

(1) Translational motion of center of gravity

The forces acting on the center of gravity of an element are the sum of the restoring and contact forces between the elements and external forces, such as gravitational force and inertial force due to an earthquake. The restoring or contact force by the spring between two certain elements in contact is obtained by multiplying the spring constant per area (Eq. (3)) by the relative displacement between the relevant elements and the area of the segment. The contact force by the dashpot between two certain elements in con-

tact is obtained by multiplying the damping coefficient per area (Eq. (4)) by the relative velocity between the relevant elements and the area of the segment. The total sum of the restoring and contact force for a certain element is obtained by summing up the restoring or contact force by springs and dashpots for all elements with which the element of interest is in contact. For more details, see [7]. The equation of motion for translational motion is written as

$$m\ddot{\mathbf{x}}_g(t) = -m\mathbf{g} - m\ddot{\mathbf{z}}(t) + \sum \mathbf{F}(t), \tag{10}$$

where $\mathbf{x}_g(t)$ is the displacement vector of the center of gravity of an element at time $t$, $m$ is the mass of the element, $\mathbf{g}$ is the gravitational acceleration vector, is the ground acceleration vector, and $\Sigma\mathbf{F}(t)$ is the sum of the restoring and contact force vectors at time $t$.

From Eq. (10), the acceleration of the center of gravity of an element is obtained, and the velocity and displacement are then obtained by integrating the acceleration. Therefore, the coordinates of the center of gravity of an element can be traced.

(2) Rotational motion around the center of gravity

The angular velocity vector in an inertial coordinate system is obtained by solving the following Eulerian equation of motion:

$$\mathbf{I}\dot{\boldsymbol{\omega}}(t) + \boldsymbol{\omega}(t) \times \mathbf{I}\boldsymbol{\omega}(t) = \sum \mathbf{R}(t)\mathbf{r}(t) \times \mathbf{R}(t)\mathbf{F}(t), \tag{11}$$

where $\mathbf{I}$ is the tensor of the inertial moment, $\mathbf{r}(t)$ is the vector in the absolute coordinate system between the center of gravity and the point at which $\mathbf{F}(t)$ acts, and $\mathbf{R}(t)$ is the matrix representing the transformation from the absolute coordinate system to the inertial coordinate system.

The vector from center of gravity $\mathbf{x}_g(t)$ to arbitrary point $\mathbf{x}_p(t)$, $\mathbf{x}_{gp}(t)$, is obtained by integrating the velocity obtained in the following equation:

$$\dot{\mathbf{x}}_{gp}(t) = (\mathbf{R}^T(t)\boldsymbol{\omega}(t)) \times \mathbf{x}_{gp}(t), \tag{12}$$

where $\boldsymbol{\omega}(t)$ on the right-hand side is the angular velocity vector in the inertial coordinate system, obtained by solving Eq. (11).

The coordinates of arbitrary point $\mathbf{x}_p(t)$ are obtained as follows by using $\mathbf{x}_{gp}(t)$ in Eq. (12):

$$\mathbf{x}_p(t) = \mathbf{x}_g(t) + \mathbf{x}_{gp}(t). \tag{13}$$

The coordinates of the arbitrary point on the element can be traced by solving Eqs. (11)-(13) step by step.

### 2.6 Stability condition of solution

In this study, the leap-frog method is applied as a time integration scheme to solve the equation of motion. In the leap-frog method, the stability condition of the solution is written as

$$\Delta t < \sqrt{m / K_n}. \tag{14}$$

From Eqs. (2), (4), and (14), the stability condition for translational motion is determined by [9].

$$\Delta t \le \sqrt{\rho \ell^2 (1 - \nu^2) / E}. \tag{15}$$

## 3.Proposed method (Deformable DEM)

### 3.1 Basic concepts

This study proposes a new element model to consider the deformation of an element itself. In the new element model (**Fig. 4**), an element is divided into two parts. An inner part (deformation part) considers deformation of the element itself, and an outer part (contact part) deals with contact between elements. The deformation part is modeled as an elastic FEM element. The stiffness matrix of an eight-node solid element is used to obtain the restoring force due to deformation. The contact part is assumed to move along the deformation part with a constant thickness. Then, the coordinates of the vertices of an element are determined by the coordinates of nodes of a FEM element. In the new DEM, the behavior of each node is tracked step by step. The concept of the refined DEM is applied so as to consider the contact between elements. Then, a restoring spring is set between continuous elements prior to mortar failure, and a contact spring and a contact dashpot are attached between elements when they are in contact or recontact. It is desirable that the thickness of the contact part is set to be as thin as possible, to obtain high accuracy.

In the new DEM, structural deformation is expressed by the sum of the deformation of elements and the contact between elements. Then, the forces acting on a node are the sum of external forces (e.g., gravity and inertia), restoring and contact forces be-

tween elements, and reaction forces that oppose element deformation. The coordinates of each node are obtained by solving the equation of motion for each node. Therefore, the behavior of the structure is traced by tracking the behaviors of each node, step by step.

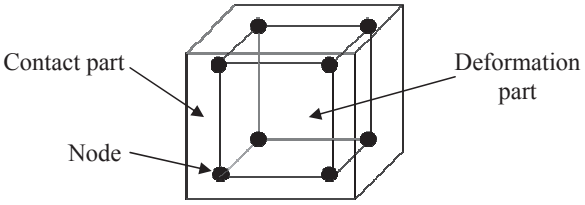


**Figure 4.** New element model

### 3.2 Analytical parameters

(1) Contact part

The analytical parameters in the contact part are the spring constants of the restoring and contact springs and the damping constant of the contact dashpot.

The values used for the restoring and contact springs are the same as for the refined DEM. The spring constants of the spring between elements, A and B, are written as follows by referring to Eq. (2):

$$\bar{k}_n = \frac{1}{\frac{r_A - t_M/2}{E_A/(1-\nu_A^2)} + \frac{t_M}{E_M/(1-\nu_M^2)} + \frac{r_B - t_M/2}{E_B/(1-\nu_B^2)}}, \text{ and}$$

$$\bar{k}_s = \frac{1}{\frac{r_A - t_M/2}{E_A/2(1+\nu_A)} + \frac{t_M}{E_M/2(1+\nu_M)} + \frac{r_B - t_M/2}{E_B/2(1+\nu_B)}}, \quad (16)$$

where $r_A$ and $r_B$ are the thicknesses of the contact parts in elements A and B.

The damping constant is determined by substituting $\overline{k_n}$ and $\overline{k_s}$ into Eq. (4).

(2) Deformation part

A stiffness matrix for the 3D FEM is introduced in the deformation part. This study applies an eight-node hexahedral element. Letting **K** be the element stiffness matrix, **u**($t$) be the relative displacement vector at time $t$, and $\mathbf{f}_{react}(t)$ be the vector of reaction force against deformation, $\mathbf{f}_{react}(t)$ is then written as

$$\mathbf{f}_{react}(t) = \mathbf{K}\mathbf{u}. \quad (17)$$

### 3.3 Equations of motion

(1) Translational motion of the center of gravity and rotational motion around the center of gravity

As with the refined DEM, the coordinates of the center of gravity and rotation around the center of gravity are obtained by solving two equations: Newton's equation for translational motion and Euler's equation for rotational motion around a center of gravity. Then, the coordinate axes of the element coordinate system are updated. Reaction force against deformation is not considered at this point.

(2) Motion of the node of deformation

The forces acting on each node are the sum of external forces, restoring and contact forces between elements, and reaction force against deformation. The coordinates of each node are obtained by solving the equations of motion.

Let $\mathbf{x}_{in}$ and $m_{in}$ be the relative displacement vector and the mass of a node. The subscript "*in*" indicates "inner node" since it is the node of the inner part that considers deformation of the element. The equation of motion is

$$m_{in}\ddot{\mathbf{x}}_{in}(t) = -m_{in}\mathbf{g} - m_{in}\ddot{\mathbf{z}}(t) + \sum \mathbf{f}_{contact}(t) + \sum \mathbf{f}_{deform}(t), \quad (18)$$

where $\mathbf{f}_{contact}(t)$ is the sum of restoring and contact forces acting on a node at time $t$, and $\mathbf{f}_{deform}(t)$ is the reaction forces against deformation acting on a node.

The acceleration of a node is determined by solving the equation of motion of a node. The coordinates of a node at the next time step are obtained by integrating the acceleration. The coordinates of a vertex are updated by considering the thickness of the part in contact. Then, the forces acting on a node at the next time step are also updated. In this way, the behavior of a structure can be traced by calculating the equation of motion step by step.

## 4.Numerical analysis

### 4.1 Verification of the proposed method

(1) Basic concept

This section investigates whether the proposed method can adequately model the deformation of individual elements. A vertical load is applied to an element, and the horizontal displacement is computed to confirm the appropriate simulation of Poisson's effect. The results are compared with the results obtained using the FEM.

(2) Analytical model

**Figure 5** illustrates analytical models of the proposed method and the FEM. In the proposed method, a high-density rigid element (weight $W$) was placed on a deformable element to apply the vertical load. The element is a cube measuring 0.1 m on each side and the thickness of the contact part of the element is 0.001 m.

In the FEM, a cube also measuring 0.1 m on each side was used. A load of $W/4$ was applied at each node on the upper surface of the element.

The displacement of point A (**Fig. 5**) in the $x$-direction was computed for both cases to compare the calculated displacement due to Poisson's effect.

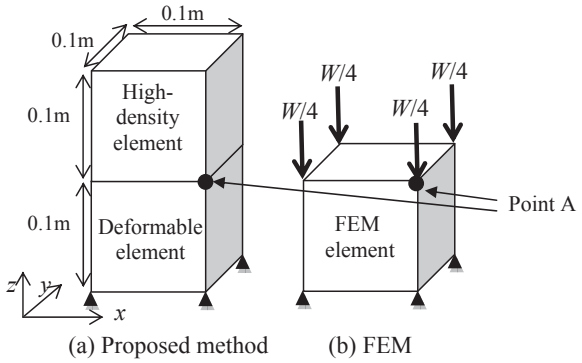


**Figure 5.** Analytical model for verification

(3) Material properties

**Table 1** presents the material properties used in the simulations. The density and Young's modulus were chosen on the basis of experimental results of adobe bricks obtained by Ghannad et al. [10] The simulation in this analysis is elastic, so the strengths of mortar (i.e., the tensile, shear, and compressive strengths) were set to have a value that was large enough not to fail. Poisson's ratio in Case 1 is 0.25, and in Case 2, it is 0.40.

**Table 1.** Material properties

| | Brick | Mortar | Rigid element |
|---|---|---|---|
| Density $p$ (kg/m$^3$) | $1.8\times10^3$ | $1.8\times10^3$ | $2.0\times10^4$ |
| Young's modulus $E$ (N/m$^2$) | $9.8\times10^7$ | | |
| Poisson's ratio $v$ | 0.25 (Case 1), 0.40 (Case 2) | | |

(4) Results

The displacement of point A (**Fig. 5**) was measured when the load in the vertical direction acted on the element. **Table 2** compares the results using the proposed method and the FEM.

In **Table 2**, the results obtained using the proposed method are found to agree well with the results of the FEM. **Figure 6** shows the deformation of the element and the displacement in the $x$-direction.

It is confirmed that Poisson's effect, which cannot be modeled by the existing DEM, was successfully expressed by the proposed method. It is also confirmed that the deformation computed by the proposed method agreed well with the FEM. In masonry buildings, bricks support the vertical gravity load of the bricks stacked above, and this vertical gravity load causes deformation in the horizontal direction due to Poisson's effect. In the following sections, the effect of this Poisson's effect is examined by comparing the results of the proposed method and the refined DEM.

**Table 2** Analysis results

| | Proposed method | FEM |
|---|---|---|
| Case 1 ( $v = 0.25$) | $6.804\times10^{-6}$ (m) | $6.802\times10^{-6}$ (m) |
| Case 2 ( $v = 0.40$) | $9.280\times10^{-6}$ (m) | $9.142\times10^{-6}$ (m) |

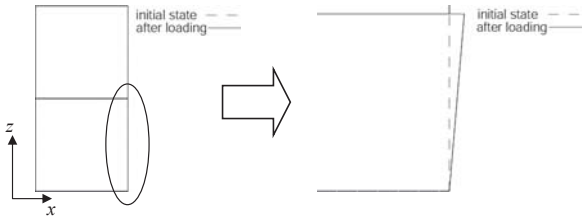


**Figure 6.** Result of this analysis (Poisson's ratio 0.40)

### 4.2 Seismic behavior analysis of a masonry wall

(1) Basic concept

Seismic analyses using the proposed method and the refined DEM were conducted by modeling the propagation of a ground motion source into a simple masonry wall. From these analyses, the effect of considering deformation is investigated.

(2) Analytical model

**Figure 7** illustrates the masonry wall models analyzed in this section. The wall has a width of 1.2 m in the $x$-direction, a depth of 0.2 m in the $y$-direction, and a height of 1.2 m in the $z$-direction. The $x$-direction is regarded as the in-plate direction, and the $y$-direction is regarded as the out-of-plate direction.

Two types of models were applied in these anal-

yses. **Figure 7 (a)** is a straight joint wall model consisting of straight joints in both the horizontal and vertical directions. **Figure 7 (b)** is referred to as an English bond wall model. The joint is straight in the horizontal direction, but not in the vertical direction. The straight joint wall model consists of cubic elements with edges of 0.2 m long. The English bond wall model consists of two types of elements: cubic elements with edges of 0.2 m long, and rectangular-parallelepiped elements of 0.1 m×0.2 m×0.2 m.

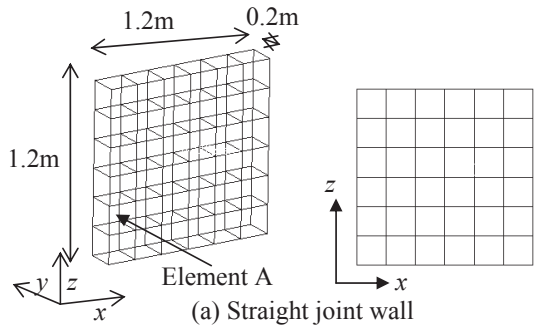


(a) Straight joint wall

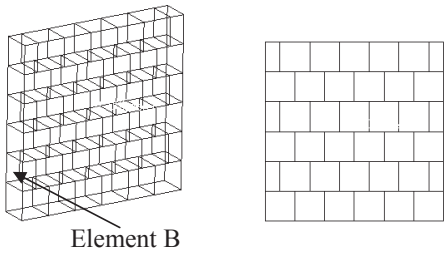


(b) English bond wall

**Figure 7.** Analytical model

(2) Material properties

**Table 3** shows the material properties of the bricks and mortar. The strengths of the mortar are based on field experimental results obtained during a survey of the damage resulting from the 2003 Bam earthquake [11].

**Table 3.** Material properties

| | Brick | Mortar |
|---|---|---|
| Density $p$ (kg/m$^3$) | $1.8\times10^3$ | $1.8\times10^3$ |
| Young's modulus $E$ (N/m$^2$) | $9.8\times10^6$ | $9.8\times10^6$ |
| Poisson's ratio $v$ | 0.25 | 0.25 |
| Tensile strength (N/m$^2$) | - | $4.6\times10^3$ |
| Shear strength (N/m$^2$) | - | $2.9\times10^3$ |
| Friction angle | - | 32° |
| Compressive strength (N/m$^2$) | - | $4.9\times10^5$ |

(3) Input ground motion

The Building and Housing Research Center in Iran recorded the unique main shock of the Bam earthquake [12]. The acceleration of the horizontal component of the earthquake is oriented in the in-plate direction (**Fig. 8**).

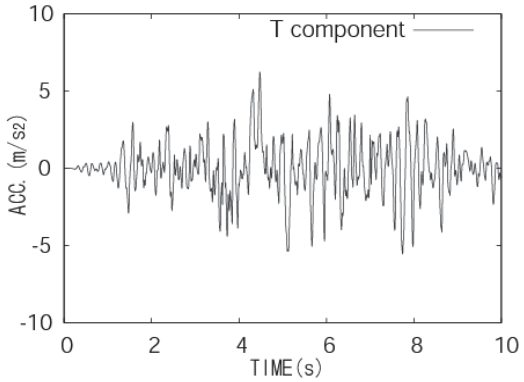


**Figure 8.** Input ground motion

### 4.3 Results

The relative displacements of the center of gravity of element A and B (**Fig. 7**) are shown in **Figs. 9** and **10**. The relative displacements from 0.0 to 1.5 s are used to compare the results of the refined DEM and the proposed method. In addition, the seismic behaviors of structures obtained by the two methods are compared. The results of the refined DEM are referred to as "RIGID" and the results of the proposed method are referred as "DEFORM".

(1) History of the relative displacement

**Figures 9** and **10** show the relative displacements from 0.0 to 1.5 s. Before initializing ground motion, a self-weight was applied to the structures. The ground motion was instigated after the structures reached a stable condition under their own weight.

a) Straight joint wall model

**Figures 9 (a)**, **(b)**, and **(c)** illustrate the relative displacements in the $x$-, $y$-, and $z$-directions, respectively. From **Fig. 9 (a)**, the amplitude obtained using the refined DEM (RIGID) is nearly 0.0 m and the amplitude obtained using the proposed method (DEFORM) is about

-0.0002 m from 0.0 to 0.3 s. These analyses were conducted after initializing the self-weight, so that the initial difference between both methods is due to Poisson's effect under this self-weight. In **Fig. 9 (b)**,

the displacement is observed to be nearly 0.0 s in RIGID because the refined DEM does not consider Poisson's effect. In comparison, Poisson's effect is observed using the DEFORM method. The differences in **Fig. 9 (a)**, **(b)**, and **(c)** are due to the deformation caused by Poisson's effect.

b) English bond wall model

**Figure 10** shows the results of an English bond wall model. Like the straight joint wall model, the difference from 0.0 to 0.3 s is due to self-weighted Poisson's effect. As shown in **Fig. 10 (b)**, the displacement in RIGID is 0.0 m, whereas Poisson's effect is observed in DEFORM. Therefore, by investigating the differences in the two methods, the proposed method is confirmed to express Poisson's effect by considering the deformation of the element.

(2) Seismic behavior

The seismic behavior of the structure at 4.0, 4.5, 5.0, 5.5, and 6.0 s is compared in this section.

a) Straight joint wall model

As shown in **Fig. 11**, failure occurs at **(a)** and the structure collapses at **(c)** in RIGID. In DEFORM, the structure collapses later than in RIGID.

This model has straight joints, so the failure spreads easily. In RIGID, compressive force due to Poisson's effect by the self-weight of horizontally adjacent elements cannot be applied because the deformation of elements is ignored. As a result, the modeled structure collapses easily. On the other hand, in DEFORM, compressive forces do act between elements because of Poisson's effect. These compressive forces work as a prestress, so that the structure is stronger and collapses later than in RIGID.

b) English bond wall model

As shown in **Fig. 12**, a crack is generated with a diagonal orientation but the structure does not collapse in RIGID. This is because the joints of an English bond wall are complicated and they enhance the interlocking between elements. In DEFORM, a large crack is generated at **(a)** and the upper part collapses at **(b)**. The elements deform in DEFORM, so that the interlocking of joints is weaker than in RIGID.

Compared with other models, the English bond wall model is strongest in RIGID. The straight joint wall model collapses easily due to the straight joint. However, the English bond wall model has complicated joints and does not readily collapse. In DEFORM, both models collapse, but the number of fallen bricks is smaller in the English bond wall model than in the straight joint wall model.

**5.Conclusions**

In this study, we propose a distinct element method that considers element deformability. The deformation of an element can be expressed by dividing the element into a deformation part and a contact part.

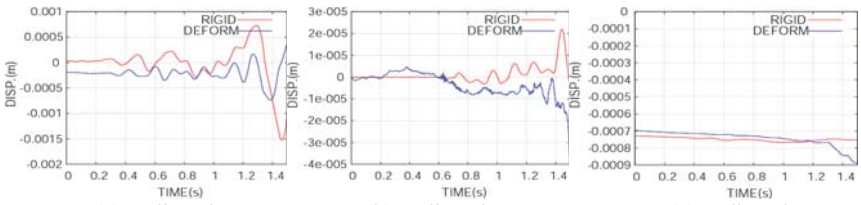


(a) *x*-direction (b) *y*-direction (c) *z*-direction

**Figure 9.** History of relative displacement (straight joint wall model)

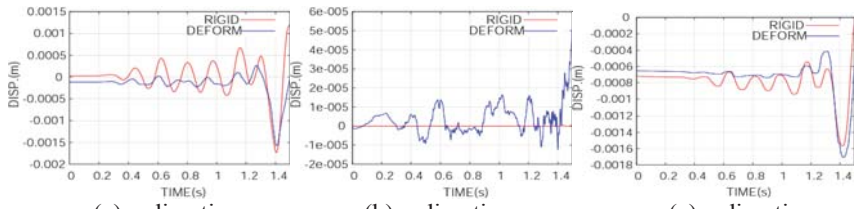


(a) *x*-direction (b) *y*-direction (c) *z*-direction

**Figure 10.** History of relative displacement (English bond wall model)

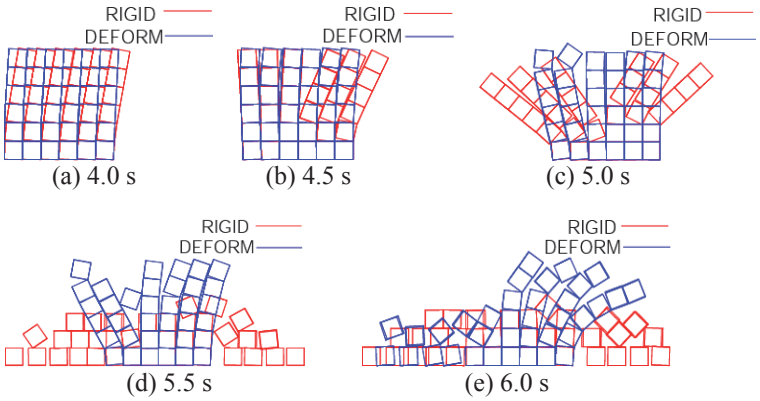


**Figure 11.** Deformation form (straight joint wall model)

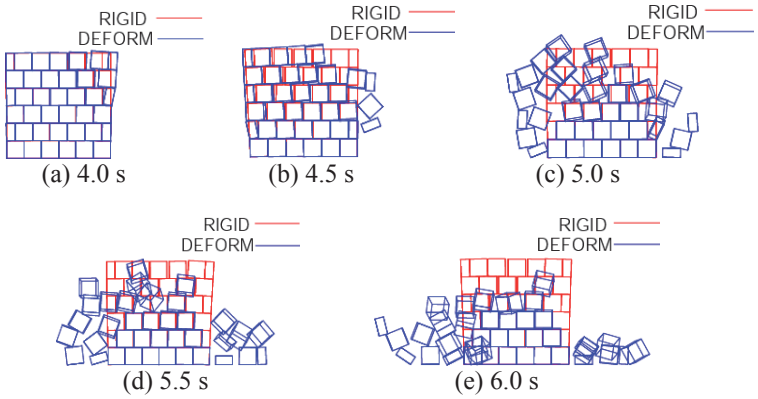


**Figure 12.** Deformation form (English bond wall model)

Horizontal displacement against the vertical load is calculated using the proposed method. The results obtained using the proposed method agree well with the results of the FEM. The proposed method is confirmed to correctly express Poisson's effect.

The seismic behaviors of simple masonry walls were simulated using the proposed method and the refined DEM. The effect of considering deformation was investigated by comparing the results of both methods. Ground motion was input in the in-plane direction. In the refined DEM, compression force due to self-weight between horizontally adjacent elements cannot be expressed, which means that a straight joint wall model collapses easily. In the proposed method, compressive forces are generated between horizontally adjacent elements because the method can consider Poisson's effect. The structure collapsed later, which is modeled better in the proposed method than in the refined DEM owing to these compressive forces. An English bond wall model collapses less easily than a straight joint model because of the interlocking effect due to the complexity of the joints. In the refined DEM, the effect of interlocking is clearly seen; however, in the proposed method, the effect is weaker as a result of element deformation.

When ground motion was input in the out-of-plane direction, the results of the two methods were almost the same, because there is only one element in the out-of-plane direction and the influence of Poisson's effect is small. In real masonry buildings, the critical failure pattern is out-of-plane failure. The seismic behavior of masonry buildings, however, is very complicated since if one wall vibrates in the out-of-plane direction, the orthogonal wall vibrates in the in-plane direction. Therefore, the authors would like to investigate the influence of element deformability by analysis through the simulation of buildings in a further study.

Since the validity of the proposed method has not been confirmed by the experiment, the authors would like to compare the analytical results with an experiment to examine the validity of the proposed method in a future study.

**Acknowledgement**

This work was supported by JSPS KAKENHI Grant Number 00380585.

**References**

[1] OCHA (Office for the Coordination of Humanitarian Affairs), http://www.unocha.org/ [Accessed: Dec, 2012].

[2] O. C. Zienkiewicz and R. L. Taylor, The finite element method, 5th edition, Vol. 1, 2, 3, Butterworth Heinemenn: Oxford, U.K., 2000.

[3] K. Oguni, M. Hori, and K. Sakaguchi, Proposal of new FEM for analysis of failure phenomena, Journal of the JSCE, No. 766/I-68, pp. 203-217, 2004.

[4] P. A. Cundall and O. D. L. Strack, A discrete numerical model for granular assemblies, Geotechnique, 29, pp. 47-65, 1979.

[5] K. Meguro and M. Hakuno, Fracture analysis of concrete structures by the modified distinct element method, Proc. of JSCE, Structural Eng./Earthquake Eng., Vol. 6, No. 2, pp. 283s-294s,1989.

[6] T. Nakagawa, T. Narafu, H. Imai, T. Hanazato, Q. Ali, and C. Minowa, Collapse behavior of a brick masonry house using a shaking table and numerical simulation based on the extended distinct element method, Bulletin of Earthquake Engineering, Vol. 10, pp. 269-283, 2012.

[7] A. Furukawa, J. Kiyono, and K. Toki, Proposal of a numerical simulation method for elastic, failure and collapse behaviors of structures and its application to seismic response analysis of masonry walls, Journal of Disaster Research, Vol. 6, No. 1, pp. 51-68, 2011.

[8] P. B. Lourenco, Analysis of masonry structures with interface elements, theory and applications, Delft University of Technology, Faculty of Civil Engineering, TU-DELFT report no. 03-21-22-0-01, 1994.

[9] U. M. Ascher and L. R. Petzold, Computer methods for ordinary differential equations and differential-algebraic equations, Society for Industrial Mathematics, 1998.

[10] M. A. Ghannad, A. Bakhshi, S. E. Mousavi Eshkiki, A. Khosravifar, Y. Bozorgnia, and A. A. Taheri Behbahani, A study on seismic vulnerability of rural houses in Iran, Proc. of the First European Conf. on Earthquake Engineering and Seismology, Paper No. 680, 2006.

[11] J. Kiyono and A. Kalantari, Collapse mechanism of adobe and masonry structures during the 2003 Iran Bam earthquake, Bulletin of Earthquake Research Institute, University of Tokyo, 79, pp. 157-161, 2004.

[12] BHRC, The very urgent preliminary report on Bam earthquake of Dec. 26, 2003. http://www.bhrc.gov.ir, 2003 [Accessed: Dec. 2012].